ACS APPLIED MATERIALS & INTERFACES

Research Article

www.acsami.org

Stimuli-Responsive Topological Change of Microstructured Surfaces and the Resultant Variations of Wetting Properties

Zi Liang Wu,*[,†] Renbo Wei,[‡] Axel Buguin,[†] Jean-Marie Taulemesse,[§] Nicolas Le Moigne,[§] Anne Bergeret,[§] Xiaogong Wang,[‡] and Patrick Keller*[,†]

[†]Institut Curie, Centre de Recherche, CNRS UMR 168, Université Pierre et Marie Curie, 26 rue d'Ulm 75248 Paris cedex 05, France

[‡]Department of Chemical Engineering, Laboratory for Advanced Materials, Tsinghua University, Beijing, 100084, China

[§]Centre des Matériaux (C2MA), Ecole des Mines d'Alès, 6 avenue de Clavières 30319 Alès cedex, France

Supporting Information

ABSTRACT: It is now well established that topological microstructures play a key role in the physical properties of surfaces. Stimulus-induced variations of topological microstructure should therefore lead to a change in the physical properties of microstructured responsive surfaces. In this paper, we demonstrate that roughness changes alter the wetting properties of responsive organic surfaces. Oriented nematic liquid crystalline elastomers (LCEs) are used to construct the microstructured surfaces via a replica molding technique. The topological microstructure of the surfaces covered with micropillars changes with temperature, due to the reversible contraction of the LCE pillars along the long axis at the nematic-to-isotropic phase transition. This is directly observed for the first time under environmental scanning electron microscopy (E-SEM). A high boiling point liquid, glycerol, is used to continuously monitor the contact angle change with temperature. The glycerol contact angle of the microstructured surfaces covered with small pillars decreases from 118° at room temperature to 80° at 140 °C, corresponding to a transition from Cassie state to Wenzel state.

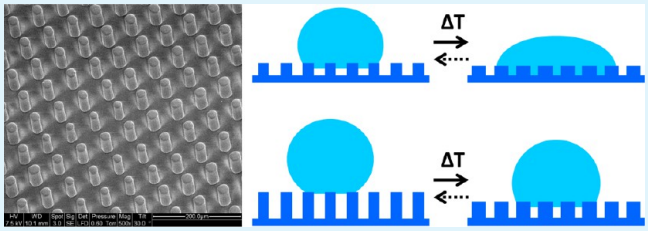

KEYWORDS: *wetting properties, microstructured surfaces, liquid crystalline elastomers, topological structure change, responsive surfaces, Cassie−Wenzel transition*

INTRODUCTION

Nature has produced numerous microstructured surfaces with robust functions, serving as excellent paradigms for creating artificial functional systems.[1−4] As a famous example, the surface of the lotus leaf has many micropapillae covered with hydrophobic epicuticular wax, endowing it with superhydrophobicity and self-cleaning capacity.[3] The foot pads of gecko are composed of thousands of keratinous foot-hairs named setae, which contain hundreds of submicrometer-size terminal spatula; this specific structure effectively produces adhesive force and enables geckos to cling to smooth vertical surfaces and climb rapidly.[2] The literature abounds in examples reporting the creation of biomimetic structured surfaces with special wetting properties, remarkable iridescent colors, controllable adhesives properties, etc.[3−11] Some of the functions of artificial surfaces go even beyond those developed in nature, such as reversible transformation between superhydrophobic and superhydrophilic states.[12−18] For example, the wetting properties of ZnO nanorod film could be switched by exposing the surface to UV light/in the dark, corresponding to hydrophilic or hydrophobic surfaces with hydroxyl groups or oxygen vacancies, respectively.[14] The water contact angle of a structured surface coated with a responsive poly(*N*-isopropylacrylamide) brush can be tuned by temperature.[16] In these systems, the switching usually results from changes in the chemical properties of the surfaces constructed from responsive polymers or inorganic nanomaterials.

On the other hand, it is well established that topological microstructure plays a key role in the determination of the physical properties of a surface.[19,20] Thus, in situ variation of the surface microstructure should result in changes of the surface properties. Recently, Chuang et al. reported that the wetting properties of a wrinkled surface made of a polymer changed with the wavelength and amplitude of the wrinkles, which was mediated by the compressive strain.[21,22] To construct surfaces with modifiable topographic microstructures, responsive soft material such as liquid crystalline elastomers (LCEs), which show stimuli-triggered reversible, anisotropic contraction and have been used to prepare macro- and microactuators,[23−28] could be among the best candidates. Zeng et al. revealed that the light-induced contraction of azobenzene-containing LCE micropillar arrays along their long axis suppressed the light reflection behavior of the surface.[29]

Received: May 13, 2013
Accepted: July 12, 2013
Published: July 12, 2013

   dx.doi.org/10.1021/am4017957 | *ACS Appl. Mater. Interfaces* 2013, 5, 7485−7491

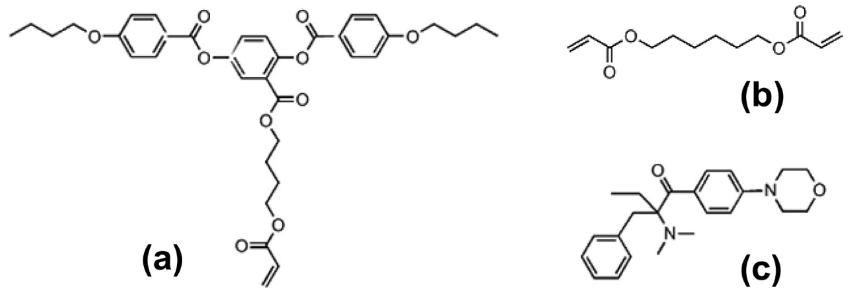

Figure 1. Chemical structures of the reagents used for preparation of liquid crystalline elastomers: (a) the monomer A444, (b) the chemical cross-linker, and (c) the photoinitiator.

Our recent work also demonstrated that a roughness change could result in a transition between Cassie and Wenzel states for a water drop sitting on a surface covered with LCEs micropillars.[30] For this experiment, we prepared a LCE with a low nematic-to-isotropic transition temperature, T_{NI}, of 76 °C and contraction of around 34%; The LCE was made from 3″-vinylcarbonyloxypropyl 2,5-di(4′-octyloxybenzoyloxy)benzoate, a side-on nematic monomer, and the surface was covered with micropillars by using the replica molding technique. Due to the relatively low T_{NI} of the elastomer, we were able to study the water contact angle change as a function of the temperature for the microstructured surface up to the isotropic phase of the LCE. However, we noticed a poor reversibility of the water contact angle measured at room temperature after several heating (pillar contraction)-cooling (pillar extension) cycles, which we attributed to the weak mechanical properties of the elastomer.[30] In addition, the measurements of water contact angle at a specific temperature had to be conducted within a short time (less than 20 s) to avoid solvent evaporation, especially when the temperature was close to the T_{NI}. To further reveal the relationship between topological microstructure change and variation in wetting properties, it is important to directly observe the topological microstructures of the surface and continuously monitor the contact angle change for a unique drop during the whole heating/cooling process.

In the present paper, we study the topological-change-mediated wetting properties of microstructured LCE surfaces made from a typical liquid crystalline (LC) monomer, 4″-acryloyloxybutyl 2,5-di(4′-butyloxybenzoyloxy)benzoate (A444). This side-on nematic LCE elastomer, despite its high T_{NI}, is tougher than the one made from carbonate LC monomer, so that the topological structure of micropillars is well maintained after peeling off the mold.[31] Both biomimetic and purely artificial microstructured responsive surfaces are studied. We use for the first time environmental scanning electron microscopy (E-SEM) to observe in situ the behavior of the structured surfaces under heating−cooling cycles and confirm the changes of topology. Furthermore, glycerol is used as the liquid to characterize the wetting properties (contact angle (CA) measurements) of the surfaces. Glycerol has a high boiling point and a surface energy close to that of water, making it an ideal substitute for water in monitoring CA changes with temperature for high T_{NI} LCEs. The relationships between the variations of topological structure and the wetting properties of the microstructured surfaces are discussed.

EXPERIMENTAL SECTION

The LC monomer A444 was synthesized as described eleswhere.[32] 1,6-Hexanediol diacrylate (chemical cross-linker; Sigma-Aldrich) and 2-benzyl-2-(dimethylamino)-4′-morpholinobutyrophenone (photoinitiator; Sigma-Aldrich) were used as purchased. The chemical structures of the reagents are shown in Figure 1.

A mixture of A444 monomer (90 mol %), cross-linker (10 mol %), and initiator (0.2 mol % of the total reactants) was used in the preparation of monodomain LCE films and biomimetic/artificial microstructured surfaces. For monodomain LCE films, the mixture, heated to 95 °C in its isotropic phase, was filled by capillarity in rubbed polyimide-coated glass cells of 20 μm gap (commercial Instec LC cells). The filled cells were slowly cooled down at −1 °C/min to 62 °C, the nematic phase of the mixture, to achieve planar alignment of the mesogens. Subsequently, UV irradiation (365 nm, 30 mW/cm^2)-initiated polymerization was carried out for 30 min. The free-standing, monodomain LCE films were obtained by dissolving the glass cells with 40% aqueous hydrofluoric acid solution. The microstructured LCE surfaces were fabricated by using a replica molding technique.[31,33] The PDMS soft molds, replicating the lotus leaf and rice leaf surfaces, and the molds with microhole arrays were prepared by using a soft-lithography technique.[34] A small amount of reactant mixture was heated to 95 °C on a microscope slide positioned atop a permanent magnet (1 T NdFeB rare earth magnet). Then, the mold was gently pressed down on the melted sample, which filled the inner structure of the mold. The temperature was then slowly decreased (−1 °C/min) to 62 °C. During the cooling process, the applied magnetic field ensured the alignment of the nematic director perpendicular to the LCE surface. The sample was then irradiated through the mold using a UV lamp for 30 min. After cooling to room temperature, the PDMS mold was peeled off, leaving a thin glassy polymer film with biomimetic/artificial microstructures on its surface.

The contractions of macroscopic LCE films and micrometer-sized pillars were measured by the dimension change of the samples in the alignment direction of side-on mesogens. The contraction was calculated by $(L - L_0)/L_0$, in which L and L_0 are the length of the samples at room temperature and above T_{NI}, respectively. The scanning electron microscopy (SEM) images were obtained at a specific temperature for samples tilted at a 30° angle, on a Quanta 200 FEG high-resolution environmental scanning electron microscope (E-SEM; FEI company). The temperature of sample holder inside the chamber could be tuned, permitting in situ observation of the surface at different temperatures. We used Image J software to analyze the diameter change of the micropillars from the SEM images. Contact angles (CAs) of the responsive surfaces at given temperatures were measured on a Digidrop contact angle meter (GBX, France). Four μL of Milli-Q water or glycerol droplets was put gently onto the surfaces of LCEs, which were gradually heated or cooled by a home-built thin hot plate. The error limits are the standard deviation values calculated from three measurements.

RESULTS AND DISCUSSION

The monodomain LCE films synthesized from A444 showed a reversible temperature-stimulated contraction along the alignment direction of the mesogens.[32] When 10 mol % cross-linker was used, the obtained LCE films had a T_{NI} of ∼125 °C (Figure S1, Supporting Information) and a contraction of ∼35% (Figure S2, Supporting Information). Using a replica molding

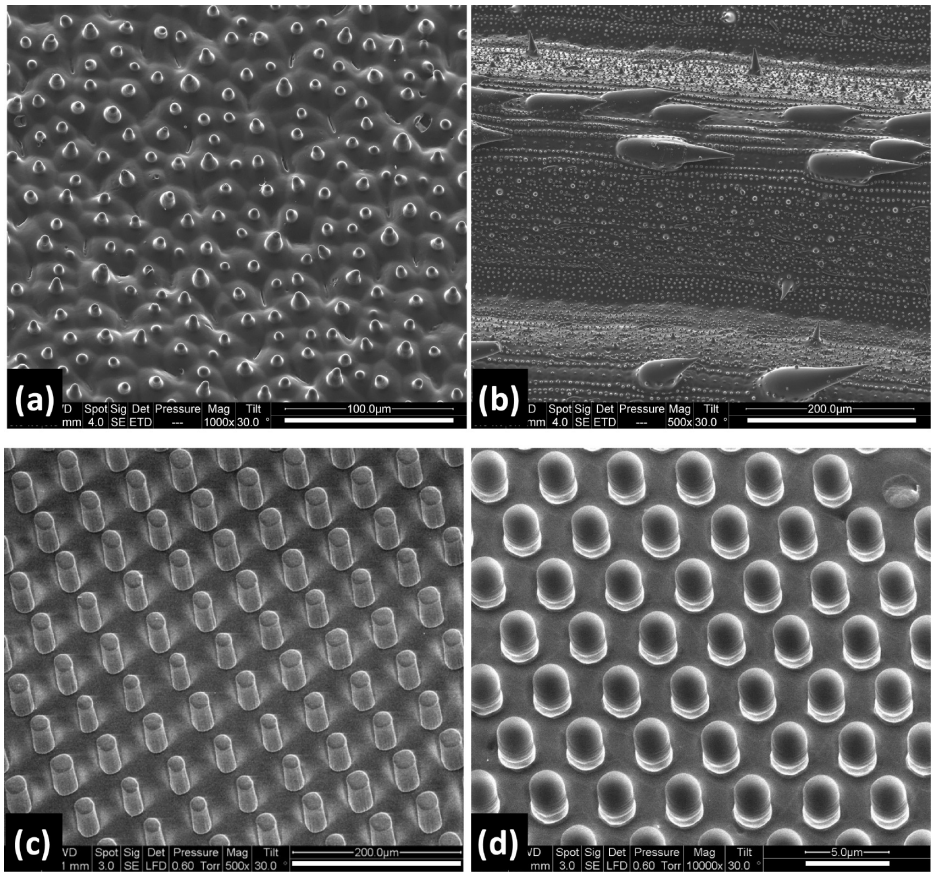

Figure 2. SEM images of the liquid crystalline elastomer surfaces of lotus leaf replica (a), rice leaf replica (b), and microstructured surfaces covered with pillars (c,d). Micropillar dimensions: (c) diameter, 20 μm; height, 100 μm; spacing, 60 μm (cubic arrangement); (d) diameter, 3 μm; height, 4 μm; spacing, 4.5 μm (hexagonal arrangement). Scale Bars: (a) 100 μm; (b,c) 200 μm; (d) 5 μm.

technique, biomimetic/microstructured surfaces were prepared. Figure 2a shows that the biomimetic surface of a natural lotus leaf maintained the typical structure of randomly distributed micropapillae. The replicated rice leaf surface also preserved typical microstructures, where micrometer-sized papillae similar to those of lotus leaf were segregated in quasi-one-dimensional order by prominent ridges, i.e., the veins of rice leaf (Figure 2b).[3] Water contact angle (WCA) measurements showed that the biomimetic surfaces have similar wetting properties in comparison with those of natural surfaces.[34] The replicated lotus leaf surface has a WCA of 120°; the replicated rice leaf surface shows anisotropic wettability, with WCAs parallel and perpendicular to the ridges of 107° and 126°, respectively (Table 1).

As a general approach, surfaces covered with micropillar arrays have been used to mimic natural microstructured surfaces, especially since the development of soft lithography techniques.[5,6,32,33,35] For these surfaces, the dimensions of micropillars are easily tuned for a better study of the effect of microstructures on the physical properties of the bulk surfaces.[36−38] In the present study, two kinds of micropillar-covered surfaces were fabricated with pillar dimensions of diameter = 20 μm, length = 100 μm, and spacing = 60 μm (Figure 2c; the sample was noted as D20H100) and diameter = 3 μm, length = 4 μm, and spacing = 4.5 μm (Figure 2d; the sample was noted as D3H4). The micropillars on the surfaces had good cylindrical shapes, when compared to the microstructures of surfaces prepared from LCEs of vinyl carbonate monomers.[30] The LCE of A444 has a relatively high rigidity (i.e., elastic modulus) at room temperature, which prevents shape deformations of the micropillars during the process of peeling off the mold.

Table 1. Contact Angle of Water and Glycerol on Several Kinds of Surfaces Made of A444 LCE

	contact angle (deg)	
sample	water	glycerol
lotus leaf replica	120 ± 1	113 ± 2
rice leaf replica[a]	107 ± 2 (//)	100 ± 1 (//)
	126 ± 1 (⊥)	124 ± 1 (⊥)
D3H4	127 ± 2	119 ± 1
D20H100	146 ± 1	148 ± 3
flat surface	88 ± 1	82 ± 1

[a]Rice leaf and its replica surface show anisotropic wetting properties. The contact angles parallel and perpendicular to the prominent ridges (contact lines are parallel and perpendicular to the ridges, respectively; noted as // and ⊥) are different.

The pillars on D20H100 surface were cut off by a thin razor blade and observed by polarizing optical microscopy. From this in situ observation, we see that the micropillars have a large contraction with good reversibility (Figure 3a−d). The contraction, up to ∼70% (Figure 3e), was much larger than that found for monodomain LCE film (∼35%), due perhaps to the fact that the magnetic field was more efficient than rubbed polymer surfaces in aligning the mesogens. Although the micropillars of D3H4 could not be easily cut from the surface because of the small size, we can assume that the temperature-

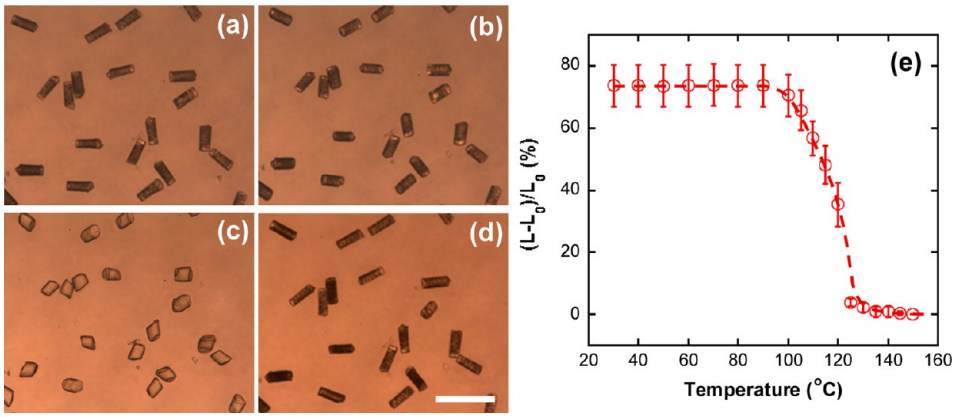

Figure 3. (a–d) Micrographs of pillars observed at different temperatures; (a) 40 °C, (b) 110 °C, (c) 130 °C, and (d) 40 °C (cooled from 130 °C). The pillars were cut off from the structured surfaces D20H100 and suspended in silicone oil to observe the shape change with temperature with a polarizing optical miscroscope. Scale bar: 200 μm. (e) Plot of contraction/expansion, $(L - L_0)/L_0$, of pillars along their long axis as a function of temperature.

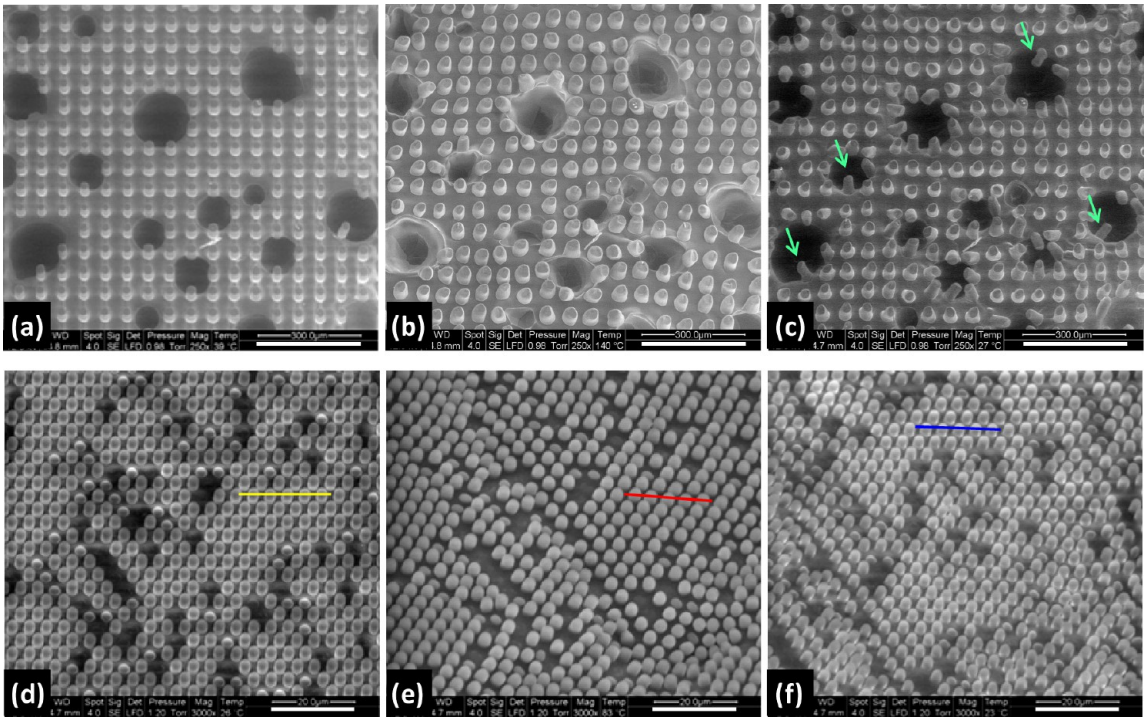

Figure 4. E-SEM images of the microstructured surface of D20H100 (a–c) and D3H4 (d–f) at different temperatures; (a,d) fresh surface at room temperature, (b,e) heated to 140 °C, and (c,f) cooled back to room temperature. Arrows in (c) show the micropillars around the cavity that show a better recovery to their original shape. The colored lines in (d–f) were used for the intensity profile (Figure 5a) to measure the diameter of the micropillars. Scale Bars: (a–c) 200 μm; (d–f) 20 μm.

stimulated contraction was similar to that of D20H100 pillars. In all cases, the reversible contraction of the micropillars along their long axis should lead to a tunable roughness change of the microstructured surfaces.

E-SEM allowed us to observe in situ the topological structure changes of the prepared surfaces with temperature. When the lotus leaf replica surface was heated from room temperature to above the LCE T_{NI} (around 125 °C), some deformations of the micropapillae were observed (Figure S3, Supporting Information), although it was very difficult to quantify the change in height of the micropapillae, due to their nonuniform shapes and sizes. In contrast, for the artificial responsive surface covered with "big" pillars, at the nematic-to-isotropic (N–I) phase transition, the diameter of the D20H100 micropillars increased (Figure 4a,b), indicating a large contraction along the long axis of the pillars and therefore a considerable roughness change. However, because of the tilt of the sample in the E-SEM chamber, the length change is difficult to evaluate. After being cooled to room temperature, the microstructure of the surface did not fully return to its original state (Figure 4c), especially the basal parts of the micropillars, which had a larger diameter than the upper parts. We noticed that the pillars around a cavity (formed probably because of an air bubble trapped inside the sample) almost fully recovered. In addition, as previously stated, the pillars cut from the surface showed good reversibility (Figure 3). These results suggest that the thin LCE layer located below the pillars affects to some extent the deformation of the pillars. On the other hand, a similar study using the

dx.doi.org/10.1021/am4017957 | ACS Appl. Mater. Interfaces 2013, 5, 7485–7491

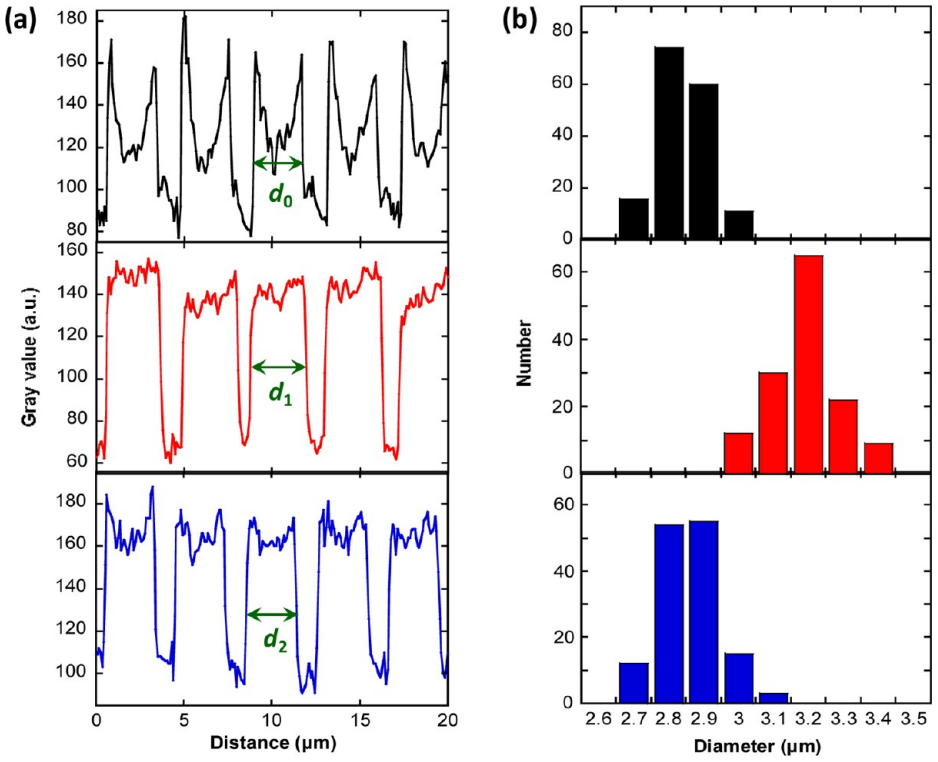

Figure 5. (a) Intensity profile along the colored lines in the SEM images in Figure 4. The diameter of D3H4 pillars was measured from the intensity profile. (b) Diameter distribution of the pillars at different temperatures. Upper, middle, and bottom figures correspond, respectively, to the SEM image (d), (e), and (f) of Figure 4.

surface covered with the small pillars (D3H4) showed that the topological structure of the surface presented a better reversibility than that of D20H100 surface (Figure 4d–f). At 140 °C, the micropillars became shorter, fatter, and more crowded on the surface.

To quantify more precisely the effect, we analyzed the diameter change of D3H4 micropillars from the SEM images. The intensity profile of the lines across an array of micropillars (marked in Figure 4d–f) clearly showed the diameter of the pillars. Compared to room temperature, the micropillars at 140 °C had a larger diameter, and at the same time, the spacing between pillars became narrower (Figure 5a). The distribution of the diameters of the micropillars at different temperatures is shown in Figure 5b. The diameter increased from d_0 = 2.85 μm at room temperature to d_1 = 3.2 μm at 140 °C and then back to d_2 = 2.87 μm after the surface was cooled back to room temperature. During the contraction process of the LCE, the diameter of the micropillars increased by around 12%, corresponding to a contraction of around 34% of the height, which is coherent with previous results.[31]

A continuous change of topological structure should result in a change in the physical properties of the surface such as wetting and adhesion.[17,18] Due to the high T_{NI} of the A444 LCE, it was not feasible to use water as the liquid to continuously measure the contact angle as a function of the temperature. We selected glycerol because it has a high boiling point, T_b ~ 290 °C, and a surface energy close to water (at 22 °C, surface energies of water and glycerol are 73 and 64 dyn/cm, respectively).[39] From Table 1, we can see that the glycerol contact angles (GCAs) for the biomimetic/artificial surfaces as well as the flat surface are similar to the WCAs.

T_b of glycerol is much higher than T_{NI} of A444 LCE, so that the solvent evaporation was avoided, allowing us to continuously observe the variation of contact angle of one drop on the surface at different temperatures. Figure 6a shows the change in GCAs of the biomimetic/artificial microstructured surfaces as a function of the temperature. A flat surface was used as the control; its GCA decreased from ~80° at room temperature to ~75° at the N–I phase transition. The GCAs for the lotus leaf replica and the D20H100 microstructured surface decreased only slightly, similar to the changes observed for the flat surface. In contrast, the GCA of the D3H4 surface clearly decreased, from ~115° at 100 °C to ~80° at 140 °C. The variations in the GCA and the contraction of the micropillars followed similar trends as the temperature increased (Figure S4, Supporting Information), indicating that the change of wetting properties was correlated with the variation of surface topological structure. Acording to the Cassie model, GCA (noted as θ^*) of the D3H4 surface at room temperature should be 140°, with $\cos\theta^* = -1 + \Phi_s(\cos\theta + 1)$,[40] in which Φ_s is the area fraction of the asperities and θ is the GCA of the flat surface (here Φ_s = 0.2, θ = 82°). The calculated GCA was larger than the experimental value of ~118°, suggesting that, in addition to the tip, the upper part of the micropillars was wetted.[7] After the N–I transition, the GCA of the D3H4 surface was close to that of flat surface, indicating that the local surface with contracted micropillars approximates a fully wetted Wenzel state.

When the D3H4 sample was cooled back to room temperature, the GCA did not recover its original value. This was because glycerol was trapped in the grooves between the pillars even after the contracted pillars fully recovered. The irreversible transition from Wenzel state to Cassie state is often observed in microstructured surfaces, because for a highly rough surface the free-energy barrier from Wenzel-to-Cassie state is much higher than that from Cassie-to-Wenzel state.[41,42]

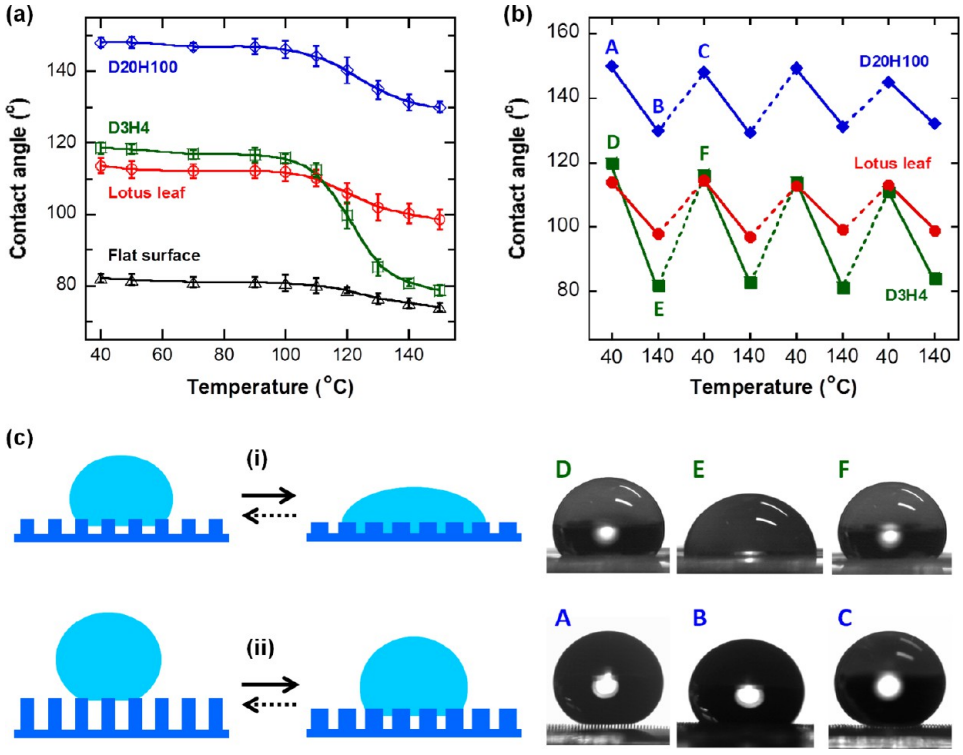

Figure 6. (a) Variation of contact angle of one glycerol drop on a responsive surface as a function of temperature during a continuous heating process. Flat LCE surface was used as the control system. (b) Cyclic measurements of the glycerol contact angle for a structured surface switching between 40 and 140 °C. After each heating process, a new glycerol drop was put on a different place of the same surface at 40 °C. (c) Schemes describing the control of the wetting properties by tuning the roughness of surfaces covered with short (i) and long (ii) micropillars. Solid and dotted lines represent the temperature-induced change of wetting properties and the return to the original state by using a new drop, respectively. The right images show the contact angles of glycerol on D3H4 (the upper images) and D20H100 (the bottom images) surfaces; A–E correspond to the points shown in panel b.

However, the GCA of a new drop on the same surface after one heating–cooling cycle had a value similar to that of a fresh surface (Figure 6c). The decrease of GCA during the heating process and recovery to its original value at room temperature when a new drop is placed on the same surface were repeatable for several cycles, indicating a good reversibility of roughness-related wetting properties (Figure 6b). For the D20H100 surface, the variation of GCA during the N–I transition was small, yet it showed reversibility similar to that of the D3H4 surface. At room temperature, the GCA of a D20H100 surface was 150°, close to the calculated θ^* of 155° (here $\Phi_s = 0.09$, $\theta = 82°$) by the Cassie model. At 140 °C, the GCA was ~130°, much larger than the 75° for the flat surface, indicating that the surface with the glycerol drop is still in Cassie state.[42] The GCA did not go back to its original value after cooling the surface to room temperature, despite the absence of the irreversible transition from Wenzel state to Cassie state. Because glycerol sticks to the LCE surface (a 4 μL glycerol drop did not slide down a flat LCE surface at a tilt angle up to 80°), the contact line between the glycerol and the tips of the micropillars did not move back even though the topological structure of the surface recovered.

We would like to point out that the topological microstructure, i.e., the dimensions of the micropillars and their spacing, is crucial in determining the wetting state of the surface. As already observed by other researchers, changing the spacing between micropillars, even though dimensions are the same, induces a change from the Cassie state to the Wenzel state.[17,37,43,44] The height of the pillars should have a similar effect.[45−47] In our systems, the D3H4 surface shows a large change of GCA as the temperature increases, which mainly originates from the decrease in height of the pillars. The change in GCA of the D20H100 surface is relatively small, although the pillars contract to a similar extent. The difference could stem from the height of pillars at high temperature, which is still too large to let the glycerol connect to the bottom surface of LCE substrate.

CONCLUSIONS

We prepared biomimetic/artificial microstructured surfaces with wetting properties at room temperature similar to those of the natural surfaces of lotus leaf and rice leaf. Due to the anisotropic deformation of LCE, the topological structure of surfaces covered with micropillar arrays changed with temperature, which was directly observed in situ by E-SEM. The microstructured surface covered with small pillars, D3H4, showed good reversible change of topological structure; micropillars had a contraction of ~35% in height and an expansion of ~12% in diameter. We used glycerol, a high boiling point liquid, to avoid solvent evaporation and continuously measured the contact angle change with temperature. This topological structure change led to a decrease of glycerol contact angle from ~115° at 90 °C to ~80° at 140 °C, corresponding to a transition from Cassie state to Wenzel state of the surface when the LCE undergoes the N–I phase transition. Although the transition from Wenzel state to Cassie state is irreversible when the sample is cooled back from 140 °C to room temperature, a new drop on the same surface still

showed Cassie state due to the full recovery of the topological structure of the surface. This work clearly underlines that modifications in the topological structure of a surface can result in changes in its wetting properties. This allows for a deeper understanding of the effects of topological changes of surfaces on their physical properties and paves the way for the design of novel functional biomimetic surfaces.

■ ASSOCIATED CONTENT

Supporting Information

DSC thermogram of LCE prepared from A444, images of LCE film to show the reversible contraction, and E-SEM images of the replicated lotus leaf surface at different temperatures. This material is available free of charge via the Internet at http://pubs.acs.org.

■ AUTHOR INFORMATION

Corresponding Author

*E-mail: ziliang.wu@curie.fr (Z.L.W.); patrick.keller@curie.fr (P.K.).

Notes

The authors declare no competing financial interest.

■ ACKNOWLEDGMENTS

This research was supported by ANR (ANR-10-INTB-0904) and a PICS-CNRS project. We thank Dr. Julie Plastino for her critical reading of the manuscript and Dr. Min-Hui Li and Dr. Vincent Semetey for their help with DSC and contact angle measurements, respectively.

■ REFERENCES

(1) Vukusic, P.; Sambles, J. R. *Nature* **2003**, *424*, 852−855.
(2) Autumn, K.; Liang, Y. A.; Hsieh, S. T.; Zesch, W.; Chan, W. P.; Kenny, T. W.; Fearing, R.; Full, R. J. *Nature* **2000**, *405*, 681−685.
(3) Sun, T.; Feng, L.; Gao, X.; Jiang, L. *Acc. Chem. Res.* **2005**, *38*, 644−652.
(4) Liu, M.; Zheng, Y.; Zhai, J.; Jiang, L. *Acc. Chem. Res.* **2010**, *43*, 368−377.
(5) Lee, H.; Lee, B. P.; Messersmith, P. B. *Nature* **2007**, *448*, 338−341.
(6) Geim, A. K.; Dubonos, S. V.; Grigorieva, I. V.; Novoselov, K. S.; Zhukov, A. A.; Shapoval, S. Y. *Nat. Mater.* **2003**, *2*, 461−463.
(7) Roach, P.; Shirtcliffe, N. J.; Newton, M. I. *Soft Matter* **2008**, *4*, 224−240.
(8) Lai, Y.; Pan, F.; Xu, C.; Fuchs, H.; Chi, L. *Adv. Mater.* **2013**, *25*, 1682−1686.
(9) Cui, J.; Drotlef, D.-M.; Larraza, I.; Fernández-Blázquez, J. P.; Boesel, L. F.; Ohm, C.; Mezger, M.; Zentel, R.; del Campo, A. *Adv. Mater.* **2012**, *24*, 4601−4604.
(10) Drotlef, D.-M.; Stepien, L.; Kappl, M.; Barnes, W. J. P.; Butt, H.-J.; del Campo, A. *Adv. Funct. Mater.* **2013**, *23*, 1137−1146.
(11) Zhao, Y.; Xie, Z.; Gu, H.; Zhu, Z.; Gu, Z. *Chem. Soc. Rev.* **2012**, *41*, 3297−3317.
(12) Xia, F.; Zhu, Y.; Feng, L.; Jiang, L. *Soft Matter* **2009**, *5*, 275−281.
(13) Lim, H. S.; Kwak, D.; Lee, D. Y.; Lee, S. G.; Cho, K. *J. Am. Chem. Soc.* **2007**, *129*, 4128−4129.
(14) Feng, X.; Feng, L.; Jin, M.; Zhai, J.; Jiang, L.; Zhu, D. *J. Am. Chem. Soc.* **2004**, *126*, 62−63.
(15) Malm, J.; Sahramo, E.; Karppinen, M.; Ras, R. H. A. *Chem. Mater.* **2010**, *22*, 3349−3352.
(16) Sun, T.; Wang, G.; Feng, L.; Liu, B.; Ma, Y.; Jiang, L.; Zhu, D. *Angew. Chem., Int. Ed.* **2004**, *43*, 357−360.
(17) Li, C.; Guo, R.; Jiang, X.; Hu, S.; Li, L.; Cao, X.; Yang, H.; Song, Y.; Ma, Y.; Jiang, L. *Adv. Mater.* **2009**, *21*, 4254−4258.
(18) Li, C.; Zhang, Y.; Ju, J.; Chen, F.; Liu, M.; Jiang, L.; Yu, Y. *Adv. Funct. Mater.* **2012**, *22*, 760−763.
(19) Persson, B. N. J.; Albohr, O.; Tartaglino, U.; Volokitin, A. I.; Tosatti, E. *J. Phys.: Condens. Matter* **2005**, *17*, R1.
(20) Peressadko, A. G.; Hosoda, N.; Persson, B. N. J. *Phys. Rev. Lett.* **2005**, *95*, 124301.
(21) Chuang, J. Y.; Youngblood, J. P.; Stafford, C. M. *Soft Matter* **2007**, *3*, 1163−1169.
(22) Zhao, S.; Xia, H.; Wu, D.; Lv, C.; Chen, Q.-D.; Ariga, K.; Liu, L.-Q.; Sun, H.-B. *Soft Matter* **2013**, *9*, 4236−4240.
(23) Ikeda, T.; Mamiya, J.; Yu, Y. *Angew. Chem., Int. Ed.* **2007**, *46*, 506−528.
(24) Lee, K. M.; Bunning, T. J.; White, T. J. *Adv. Mater.* **2012**, *24*, 2839−2842.
(25) Li, M.-H.; Keller, P. *Trans. R. Soc. A* **2006**, *364*, 2763−2777.
(26) Ohm, C.; Brehmer, M.; Zentel, R. *Adv. Mater.* **2010**, *22*, 3366−3387.
(27) Yang, H.; Ye, G.; Wang, X.; Keller, P. *Soft Matter* **2011**, *7*, 815−823.
(28) Fleischmann, E.-K.; Liang, H.-L.; Kapernaum, N.; Giesselmann, F.; Lagerwall, J.; Zentel, R. *Nat. Commun.* **2012**, *3*, 1178.
(29) Yan, Z.; Ji, X.; Wu, W.; Wei, J.; Yu, Y. *Macromol. Rapid Commun.* **2012**, *33*, 1362−1367.
(30) Wu, Z. L.; Buguin, A.; Yang, H.; Taulemesse, J.-M.; Le Moigne, N.; Bergeret, A.; Wang, X.; Keller, P. *Adv. Funct. Mater.* **2013**, *23*, 3070−3076.
(31) Buguin, A.; Li, M.-H.; Silberzan, P.; Ladoux, B.; Keller, P. *J. Am. Chem. Soc.* **2006**, *128*, 1088−1089.
(32) Thomsen, D. L., III; Keller, P.; Naciri, J.; Pink, R.; Jeon, H.; Shenoy, D.; Ratna, B. R. *Macromolecules* **2001**, *34*, 5868−5875.
(33) Yang, H.; Buguin, A.; Taulemesse, J.-M.; Kaneko, K.; Méry, S.; Bergeret, A.; Keller, P. *J. Am. Chem. Soc.* **2009**, *131*, 15000−15004.
(34) Xia, Y.; Whitesides, G. M. *Angew. Chem., Int. Ed.* **1998**, *37*, 550−575.
(35) Liu, K.; Jiang, L. *Nano Today* **2011**, *6*, 155−175.
(36) Yoshimitsu, Z.; Nakajima, A.; Watanabe, T.; Hashimoto, K. *Langmuir* **2002**, *18*, 5818−5822.
(37) Patankar, N. A. *Langmuir* **2004**, *20*, 7097−7102.
(38) Sun, T.; Wang, G.; Lin, H.; Feng, L.; Jiang, L.; Zhu, D. *J. Am. Chem. Soc.* **2003**, *125*, 14996−14997.
(39) Lange, N. A. *Handbook of Chemistry*, 10th ed.; McGrew-Hill: New York, 1967; pp 1661−1665.
(40) Callies, M.; Quéré, D. *Soft Matter* **2005**, *1*, 55−61.
(41) Lafuma, A.; Quéré, D. *Nat. Mater.* **2003**, *2*, 457−460.
(42) Ran, C.; Ding, G.; Liu, W.; Deng, Y.; Hou, W. *Langmuir* **2008**, *24*, 9952−9955.
(43) From Figure 4b, at 140 °C, the tip diameter of D20H100 pillars is approximately 30 μm, corresponding $\Phi_s \sim 0.2$ and $\theta^* \sim 138°$ by the Cassie model.
(44) Bhushan, B.; Jung, Y. C. *J. Phys.: Condens. Matter* **2008**, *20*, 225010.
(45) Reyssat, M.; Yemans, J. M.; Quéré, D. *Europhys. Lett.* **2008**, *81*, 26006.
(46) McHale, G.; Shirtcliffe, N. J.; Aqil, S.; Perry, C. C.; Newton, M. I. *Phys. Rev. Lett.* **2004**, *93*, 036102.
(47) Koishi, T.; Yasuoka, K.; Fujikawa, S.; Ebisuzaki, T.; Zeng, X. C. *Proc. Natl. Acad. Sci. U.S.A.* **2009**, *106*, 8435−8440.